Journal of Electroanalytical Chemistry 909 (2022) 116154

Contents lists available at ScienceDirect

Journal of Electroanalytical Chemistry

journal homepage: www.elsevier.com/locate/jelechem

Arsenic (III) detection with underpotential deposition on gold

Yifei Zhang, Danlei Li, Richard G. Compton *

Department of Chemistry, Physical and Theoretical Chemistry Laboratory, Oxford University, South Parks Road, Oxford OX1 3QZ, Great Britain, UK

ARTICLE INFO

Keywords:
Underpotential deposition
Anodic stripping voltammetry
Gold nanoparticles
Arsenic
Electroanalysis

ABSTRACT

We report a new, sensitive stripping voltammetric method for the detection of As(III) in aqueous solution using either a gold macroelectrode or a gold nanoparticle-modified glassy carbon electrode (GCE) based on the underpotential deposition (UPD) of As ad-atoms. The pre-concentration step deposits and accumulates As ad-atoms onto gold and is followed by a potential sweep to strip the ad-atoms with no interference from Cu (II) or Cl^- at either electrode. Linear responses were found for the range 0.01 μM to 0.1 μM or 0.005 μM to 0.1 μM at gold macroelectrodes and gold nanoparticle-modified electrodes, respectively. The visually clearly discernable signals recorded at 0.005 μM (0.4 ppb) on gold nanoparticle-modified electrodes suggests that this method has practical value given the WHO limit of 0.13 μM (10 ppb) for drinking water.

1. Introduction

Anodic stripping voltammetry (ASV) is a commonly used electrochemical method for electro-analysis to enhance sensitivity and to reach lower detection limits during measurements as compared to direct forms of voltammetry such as linear, cyclic, pulse or sinusoidal voltammetry where the peak currents can be limited by the rate of diffusion [1–4]. Microelectrodes, nanoelectrodes and arrays of these can moderate some of the limitations but ultimately the rate of diffusion to the electrode controls both limits of detection and sensitivity [5–7]. The merit of ASV as applied to the detection of metal ions is that the analyte is pre-concentrated via electro-reduction to deposit and accumulate the corresponding metal on the electrode; then a sweep voltammetry (linear or pulsed) is applied to re-oxidize the metal to metal ions and the resulting 'stripping' peak is used as a signal for the analytical detection. If the period of pre-concentration is prolonged, limits of detection (LOD) are correspondingly lowered. In this way, for example, ASV allows electro-analysis to meet the requirements of the WHO guidelines for drinking water in respect of arsenic [8–10], cadmium [4,11] and lead [11–13] amongst other targets.

Underpotential deposition (UPD) is the deposition of a metal in the form of a monolayer or sub-monolayer at the potentials lower than that required for the deposition of the bulk metal [14–17]. We have recently suggested the possible use of UPD in ASV as a possible means of overcoming some of the limitations of ASV seen when using the deposition of bulk metals [8]. In particular, a problem can arise when species additional to the target are present which can co-deposit with the target metal to form alloys or solid solutions. It was suggested that UPD may overcome these limitations in some cases and proof of concept was presented for the detection of Arsenic via UPD on platinum surfaces, where both platinum macroelectrodes and platinum nanoparticle modified carbon electrodes were seen to be suitable substrates. Meanwhile, the detection is free from interference by copper ions which is a notorious problem in the ASV analysis of Arsenic. In addition, the approach had good sensitivity and showed limits of detection with visibly discernible and recognisable signals within the WHO requirements. The proof-of-concept suggests UPD-ASV as an analytical method with distinct advantages in niche applications in addition to the lost cost and rapidity generically associated with electrochemical methods of analysis.

Arsenic species are highly toxic and exist both naturally and in industrial effluents [18–22]. Exposure to arsenic can cause severe health problems including cardiovascular disease and cancer [22–24]. The dominant forms of inorganic arsenic species in water are As(III) (AsO_3^{3-}) and As(V) (AsO_4^{3-}) [18–22]. As(III) species are more toxic than As(V) due to their interaction with enzymes in the human body [22–24]. Thus, it is important to detect As(III) in drinking water. There are many reported methods including atomic absorption spectrometry (AAS) [25] and inductively coupled plasma mass spectrometry (ICPMS) [26,27]. However, these instrumental methods require specialist laboratory conditions and lengthy sample preparation. Electrochemical methods including ASV methods, on the other hand, can provide sensitive and rapid detection with relative simple and cheap instrumentation [28,29]. To date, the lowest LOD for As detection in

* Corresponding author.
E-mail address: Richard.compton@chem.ox.ac.uk (R.G. Compton).

https://doi.org/10.1016/j.jelechem.2022.116154
Received 29 October 2021; Received in revised form 15 February 2022; Accepted 16 February 2022
Available online 18 February 2022
1572-6657/© 2022 The Authors. Published by Elsevier B.V.
This is an open access article under the CC BY license (http://creativecommons.org/licenses/by/4.0/).

water of 0.003 ppb has been claimed by Profumo *et al* by using cathodic stripping voltammetry (CSV) [30] and the greatest sensitivity was achieved by Xiao *et al* via Square Wave ASV (SWASV) with detection via the stripping of bulk As [31]. Particle modified electrodes (PMEs) have also been applied for arsenic detection. Notably, Hwang *et al* used Fe and Chitosan to modify screen-printed carbon electrode (SPCE) and obtained a LOD of 1.12 ppb via SWASV [32], and Nunez *et al* use graphene-modified SPCE to reach a LOD of 0.28 ppb via differential pulse ASV (DPASV) [33]. The proof of concept study in respect of ASV using UPD signals mentioned above and using Pt macroelectrodes and Pt nanoparticle-modified glassy carbon electrodes (GCEs), gave a visually observed detection limit of 4 ppb [8]. However, most of the ASV methods suffer from the interference of Cu(II) or Cl^- due to the formation of Cu-As alloys and solid solutions, [34] or, in the case of the use of UPD signals at platinum, competitive adsorption of As and Cl^- so precluding measurements in the presence of high levels of chloride [35]. Gold electrodes with the deposition of bulk As have been used for As(III) detection to reach low detection limits in the work of Xiao *et al* who used Au nanoparticles modified carbon nanotubes (AuCNTs) on [31] and of Yang *et al* who modified a GCE with Au nanoparticles and CeO_2-ZrO_2 for As(III) detection [36]. However the use of bulk As is prone to interference via alloy and/or the formation of intermetallic species. Thus, in this paper, we investigate the possible use of UPD-ASV for the analysis of As at low concentrations on gold surfaces with the aim of avoiding interference from both Cu(II) and Cl^-. The LOD in this paper is determined from visually clear signals rather than those calculated on the basis of 3σ method [32,33,37] , while the observed low detection limits acquired at both Au macroelectrodes and Au nanoparticle-modified electrodes were within the requirements for the WHO limits for drinking water with visually recognisable distinct signals seen at the lowest concentrations reported.

2. Experimental

2.1. Chemical reagents

Commercially available Au nanoparticles (5 nm in diameter, Sigma Aldrich, UK) were supplied suspended in sodium citrate solution. Copper(II) sulfate pentahydrate ($CuSO_4{\cdot}5H_2O$, 99%, Sigma Aldrich, UK), potassium chloride (KCl, 99.5%, Sigma Aldrich, UK), sodium (meta) arsenite ($NaAsO_2$, 99%, Fluka, Switzerland), and sulphuric acid (H_2SO_4, 98%, Fisher Scientific, UK) were purchased and used without any further purification. All aqueous solutions were prepared using deionized water (Milipore, UK) with a resistivity of 18.2 MΩ cm at 298 K.

2.2. Instrumentation

All electrochemical measurements were thermostatted at 298 (±0.1) K and were conducted with a standard three-electrode system in a Faraday cage. A gold macroelectrode (diameter of 1.60 ± 0.01 mm, geometric area of 0.02 cm^2, BASi, USA) or glassy carbon electrode (GCE, diameter of 3.00 ± 0.01 mm, geometric area of 0.07 cm^2, BAS technical, UK) operated as a working electrode, either a platinum wire or a carbon rod as a counter electrode and a mercury-mercurous sulfate electrode (MSE, BASi, USA) served as the reference electrode with a potential of + 0.65 V vs. standard hydrogen electrode (SHE) [2], and the solution used in the reference electrode was saturated K_2SO_4 solution (1.45 M). All electrochemical measurements were performed in 0.1 M H_2SO_4 with various concentrations of As(III), and were recorded with a μAutolab type III potentiostat (EcoChemie, NL) after degassing with nitrogen.

2.3. Preparation and characterization of Au nanoparticle-modified electrodes

The GCE was cleaned with alumina of decreasing particle sizes (1, 0.3 and 0.05 μm) on polishing pads then rinsed with deionized water. For drop casting of Au nanoparticles, 5 μL of stock Au nanoparticle suspension was drop casted onto the GCE using a micro pipette then dried with N_2 flow for around 15 min. The GCE was polished after each measurement then the Au nanoparticles were drop casted onto the cleaned GCE.

Figure 1 shows the TEM image of 5 nm gold nanoparticles. Each particle has a size of approximately 4–7 nm. The particles are capped by citrate and are dispersed in trisodium citrate solution [38], which prevents the particles from aggregation in aqueous solutions.

3. Results and discussion

In the following sections, first, the electrochemical behaviour of As (III) at Au macroelectrodes and electrodes modified with gold nanoparticles was studied in solutions containing 500 μM $NaAsO_2$ with 0.1 M H_2SO_4 using cyclic voltammetry (CV) and 10 μM $NaAsO_2$ with 0.1 M H_2SO_4. The voltammetric peaks were assigned and compared with literature and the presence of an As UPD peak noted. Next, a novel method based on anodic stripping voltammetry that reached a low detection limit of As was investigated using ASV with Au electrodes using pre-concentration by under potential deposition (UPD) of sub-monolayer quantities of As(0) atoms on the electrode surface. Finally, interference studies addressing Cu^{2+} and Cl^- recognised as common interferents with either As detection via ASV or with UPD on some substrates [35,39,40] were conducted.

4. Electrochemical responses of As(III) on Au electrodes

4.1. Cyclic voltammetry of As(III)

To examine the electrochemical behaviour of As(III), a gold macroelectrode was first employed using cyclic voltammetry and anodic stripping voltammetry. Fig. 2a illustrates the CV response of 500 μM $NaAsO_2$ in 0.1 M H_2SO_4 with a potential window from − 1.0 V to + 1.3 V (vs. MSE) at a gold macroelectrode. The voltammograms shown are all first scans recorded after electrode polishing. The start potential was + 0.6 V and the voltammogram was first scanned cathodically to – 1.0 V at a scan rate of 0.1 V s^{-1} and then scanned anodically to + 1.3 V. Three peaks were observed on the cathodic scan, labelled as peak 1, peak 2 and peak 3 (red line in Fig. 2a). Peak 1 observed at ca + 0.37 V was ascribed to the reduction of Au oxide to Au [41,42]. Peak 2 observed at ca − 0.66 V corresponds to the three-

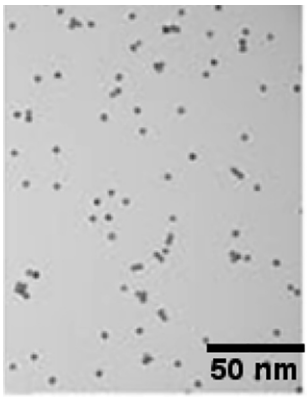

Fig. 1. TEM image of 5 nm gold nanoparticles. Reproduced with permission from Merck KGaA, Darmstadt, Germany and/or its affiliates. Ref. [38].

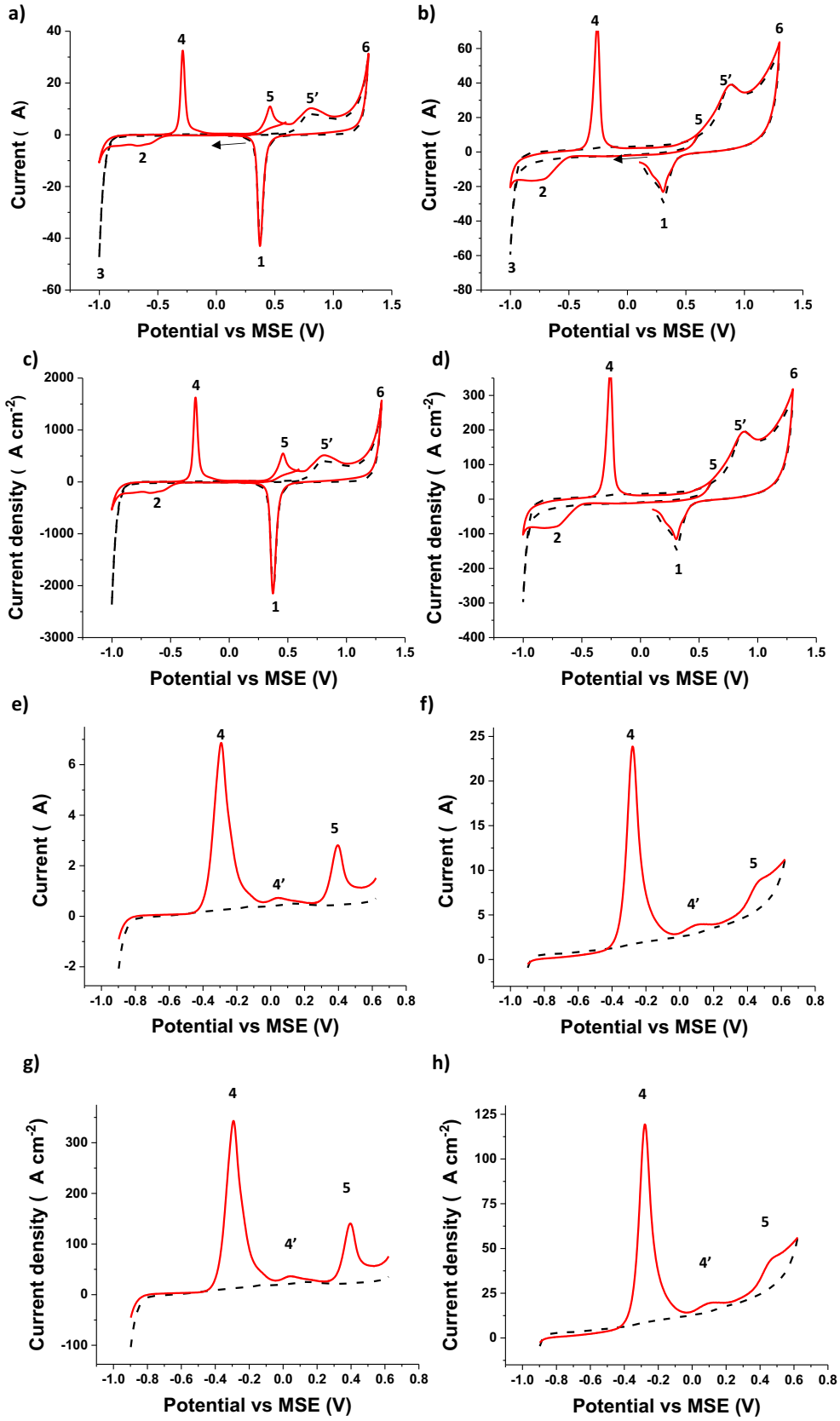

Fig. 2. CVs of 500 μM As(III) in 0.1 M H_2SO_4 (red) and blank (black dashed line) at a) and c) Au macroelectrodes, and b) and d) Au nanoparticle-modified GCEs. The voltammograms were conducted from + 0.6 V vs MSE and first scanned cathodically to − 1.0 V at a scan rate of 0.1 V s^{-1} followed by an anodic scan to + 1.3 V. The arrows represent the starting point and the direction of scan. Linear sweep voltammograms of 10 μM As(III) in 0.1 M H_2SO_4 (red) and blank (black dashed line) after pre-concentration at − 0.9 V for 300 s at e) and g) Au macroelectrodes, and f) and h) Au nanoparticle-modified GCEs. The current densities were calculated based on the currents and the estimated surface area of the gold surface (see text). The surface area of Au macroelectrode was 0.02 cm^2 and the surface area of Au nanoparticles was 0.2 cm^2 (calculation is shown on Supporting Information Section 1). LSV parameters: deposition at − 0.9 V for 300 s, scan rate was 0.1 V s^{-1}. (For interpretation of the references to colour in this figure legend, the reader is referred to the web version of this article.)

electron reduction of As(III) to As(0) [42]. Peak 3 at ca − 1.0 V represents the onset of the hydrogen evolution reaction (HER) [41]. On the reverse anodic scan, four peaks, peak 4, peak 5, peak 5′ and peak 6, were obtained. Peak 4 with the potential of ca – 0.28 V represents the re-oxidation of As(0) to the parent As(III) species [42]. Peak 5 observed at ca + 0.45 V was ascribed to the oxidation of As(III) to As(V) [41]. Another oxidation peak, peak 5′, observed at ca + 0.80 V was considered to be the oxidation of Au to Au oxide [41]. Peak 6 at ca + 1.3 V represents the start of the oxygen evolution reaction (OER) [42]. Comparing the voltammetry in Fig. 2a with that obtained in blank solution (0.1 M H_2SO_4; black dashed line in Fig. 2a), it can be seen that the three peaks (peak 2, peak 4 and peak 5) which are absent on the latter are all As(III)-related peaks, whilst peaks 1, 3, 5′ and 6 correspond to reduction of Au oxide, HER, oxidation of Au to Au oxide and OER, respectively [42]. There were three reasons to choose + 0.6 V as a starting potential. First, when choosing the starting potentials, it was necessary to scan CV cathodically initially to reduce As(III) to As(0) so that the oxidation peaks can be observed in the reverse scan. Second, the potential at +0.6 V was far from other reactions, notably the oxidation of Au (ca + 0.8 V), the reduction of Au oxide (ca + 0.35 V) and the oxidation of As(III) to As(V) (+0.45 V) (Fig. 2a and b). Third, it was also important to see if the surface of Au nanoparticles was Au or Au oxide, which is reveal by the existence or not of peak 1 during the first cathodic scan. The start potential of +0.6 V meets all these requirements.

Next cyclic voltammetry was conducted at Au nanoparticle-modified GCEs with an average coverage of 6.5×10^{-12} mol cm^{-2} corresponding to ca 1 monolayer of nanoparticles (calculations are shown in Supporting Information (SI) section 1) in a solution of 0.1 M H_2SO_4 first without the addition of arsenite. The voltammetry was conducted from +0.6 V and first scanned cathodically to – 1.0 V then scanned anodically to +1.3 V at a scan rate of 0.1 V s^{-1}. The resulting voltammetry of 0.1 M H_2SO_4 is shown in Fig. 2b (black dashed line). The peaks 1, 3, 5′ and 6 were seen at similar potentials as for Au macroelectrodes (Table 1) and assigned to the same reactions [42] as above. This was similar to that measured at the Au macroelectrodes (black dashed line in Fig. 2a).

Then the cyclic voltammetry was conducted on 500 μM As(III) in 0.1 M H_2SO_4 at Au nanoparticle-modified electrodes using a similar starting potential, potential window and sweep rate as for Fig. 2a. The resulting voltammogram is shown in Fig. 2b (red line). Seven voltammetric features were discerned at similar potentials as seen for the Au macroelectrode and assigned to the same electrochemical reactions [41,42] as above. It was noted that peak 5 is slightly different from the one in Fig. 2a. In particular whilst peak 5 can be observed clearly at Au macroelectrodes (Fig. 2) it is less well resolved at Au nanoparticle-modified GCEs (Fig. 2b) as a result of the broad width of peak 5′, which overlaps with peak 5.

Table 1
The peak potentials vs. MSE of all assigned peaks in CV and ASV at both Au macroelectrodes and Au nanoparticle-modified GCEs.

Peak number	Peak potentials at Au macroelectrodes	Peak potentials at Au nanoparticle-modified GCEs
1	+0.37 V	+0.35 V
2	−0.66 V	−0.70 V
3	−1.0 V	−1.0 V
4	−0.28 V	−0.28 V
4′ (in ASV)	+0.05 V	+0.10 V
5	+0.45 V	+0.45 V
5′	+0.8 V	+0.85 V
6	+1.3 V	+1.3 V

4.2. Deposition and stripping of As

To further understand the electrochemistry of As at gold, a 10 μM solution of $NaAsO_2$ in 0.1 M H_2SO_4 was reduced at – 0.9 V for 300 s resulting in the deposition of As(0). After deposition, a linear sweep voltammetry was conducted from – 0.9 V to + 0.62 V with a scan rate of 0.1 V s^{-1}. Fig. 2e illustrates the response at a gold macroelectrode after the pre-concentration of As(0). Three arsenic-related peaks were observed as peaks 4, 4′ and 5 (red line in Fig. 2e and 2 g). Peaks 4 and 5 observed at ca – 0.28 V and ca + 0.45 V correspond to the chemistry inferred above. The peak 4′ at ca + 0.05 V was assigned as the stripping peak associated with the oxidation of As(0) ad-atoms based on literature reports [43,44]. All three of the peaks assigned to As were absent in the blank solution (black dashed line in Fig. 2e and g).

The presence of peak 4′ in Fig. 2e presents the possibility of using anodic stripping voltammetry for analytical use based on the stripping of UPD As rather than bulk As as has hitherto been exclusively used for As. To further explore this possibility, analogous measurements were made using gold nanoparticle-modified electrodes.

Reduction of 10 μM $NaAsO_2$ in 0.1 M H_2SO_4 was carried out at – 0.9 V for 300 s to deposit As(0), then a linear sweep voltammetry was recorded from – 0.9 V to +0.62 V with a scan rate of 0.1 V s^{-1} at Au nanoparticle-modified GCEs. The voltammetric response at Au nanoparticle-modified GCEs is shown in Fig. 2f. Peaks 4, 4′ and 5 were again seen (red line in Fig. 2f) and assigned as above and elsewhere [42–44] whilst in the absence of As(III) these features disappeared (black dashed line in Fig. 2f). The voltammetric peaks showed similar peak potentials to those seen on Au macroelectrodes (Table 1). It was noted that peak 5 in ASV (Fig. 2f) is more clearly resolved than seen in CV at the Au nanoparticle-modified GCEs (Fig. 2b).

The active surface area for arsenic deposition was estimated based on either (a) the surface area of nanoparticles and assuming that the nanoparticles on the glassy carbon electrode are fully accessible or, (b) the surface area of the Au macroelectrode, which were 0.2 cm^2 and 0.02 cm^2 respectively (see calculations in SI section 1). The experimental results in Fig. 2 showed that the current on Au nanoparticles was ca 4 times higher than that at Au macroelectrodes. The reason was inferred to be partly due to the agglomeration of the drop casted Au nanoparticles, and partly due to the overlapping diffusion layers of adjacent nanoparticles. The agglomeration can reduce the active surface area of the nanoparticles whilst the diffusional overlap means that the current is not expected to scale with the particle area.

Having fingerprinted the electrochemistry using CV and ASV we next turn to investigating ASV using the UPD peak which offers likely superior analytical response as compared to cyclic voltammetry [8,40] or ASV using bulk As signals as discussed in the Introduction. The next section focuses on the detection of As using anodic stripping voltammetry with underpotential deposition on gold to approach a lower detection limit.

5. The analytical use of as UPD stripping signals

Proof of concept of using the UPD-ASV method for the detection of low concentrations of As(III) was introduced by Zhang *et al.* [8] in the specific and exclusive context of platinum electrodes. In this paper, Anodic Stripping Voltammetry is applied for the detection of As(III) in 0.1 M H_2SO_4 on both gold macroelectrodes and Au nanoparticle-modified GCEs seeking to overcome the limitations of platinum electrodes as explained in the Introduction. The pre-concentration of As (0) was first carried out at – 0.9 V for 300 s, which results in first As ad-atoms being deposited at the surface of gold [42–44] and then, in higher concentrations of As(III), bulk As on top of the ad-atoms. Then the deposited As(0) was stripped off from the electrode surface using LSV with a potential sweep conducted from –0.9 V to +0.62 V at a scan rate of 0.1 V s^{-1} and the signals were used to quantify As(III).

The signal used for the UPD-ASV analysis is the charge of peak 4′, which was calculated from the area of baseline corrected voltammogram. The procedure to obtain a baseline corrected peak 4′ is shown in SI section 2.

5.1. Observations of as UPD stripping signals

To understand and apply the As UPD signal for analytical use, experiments were first conducted in various concentrations of As(III) in 0.1 M H_2SO_4 using Au macroelectrodes. The pre-concentration of As(0) was carried out in various concentrations of As(III) at –0.9 V for 300 s followed with a linear potential sweep from –0.9 V to +0.62 V at a scan rate of 0.1 V s^{-1}. Fig. 3a illustrates the baseline corrected linear sweep voltammetric responses of peak 4′ at gold macroelectrodes measured in As(III) solutions of concentrations from 0.01 μM to 2 μM in 0.1 M H_2SO_4. The peak 4′, assigned as the stripping peak of As ad-atoms, was observed at ca + 0.05 V and the charge of the peak increased with the concentration of As(III) as shown in Table S1. The charges of peak 4′ are plotted against concentration of As(III) in Fig. 3c. The charge increases linearly to begin with before reaching a plateau consist with the formation of an estimated 0.03 layers of As ad-atoms (see SI Section 3 for calculations). The initial linear range is approximately from 0.01 μM to 0.1 μM, at which corresponds to a coverage of ca 1.0 × 10^{13} molecules cm^{-2} and 0.014 monolayers of ad-atoms (again SI section 3 for the calculations). The plateau is reached for As(III) concentrations higher than 1 μM with a corresponding surface coverage of ca 2.0 × 10^{13} molecules cm^{-2}, consistent with a sub-monolayer of As ad-atoms deposited onto the surface of Au (Table 1). This observation sets the upper limit (ca 1 μM) for detection with UPD ASV using peak 4′ at Au macroelectrodes but giving visually clear signals for concentrations as low as 0.01 μM (see SI section 4 for both raw and corrected voltammograms). To further discover the possible application of peak 4′, analogous experiments were made at Au nanoparticle-modified electrodes.

The pre-concentration of As(0) was carried out at – 0.9 V for 300 s in various concentrations of As(III) solution then followed up with a LSV from – 0.9 V to + 0.62 V at a scan rate of 0.1 V s^{-1} at Au nanoparticle-modified GCEs. The baseline correction for peak 4′ is also followed the procedure as above. Fig. 3b shows the baseline corrected LSVs of peak 4′ at Au nanoparticle-modified GCEs which was obtained from 0.01 μM to 2 μM of As(III) in 0.1 M H_2SO_4. Similar to Au macroelectrodes, peak 4′ was observed at ca + 0.1 V (Fig. 3b) and the peak charge was increased with the concentration of As(III) (Table S1). The charges of peak 4′ vs concentrations of As(III) are plotted in Fig. 3d. A similar trend is seen as observed for Au macroelectrodes reaching a limiting value of 0.87 μC (Table S1) at 0.5 μM (Fig. 3d), which corre-

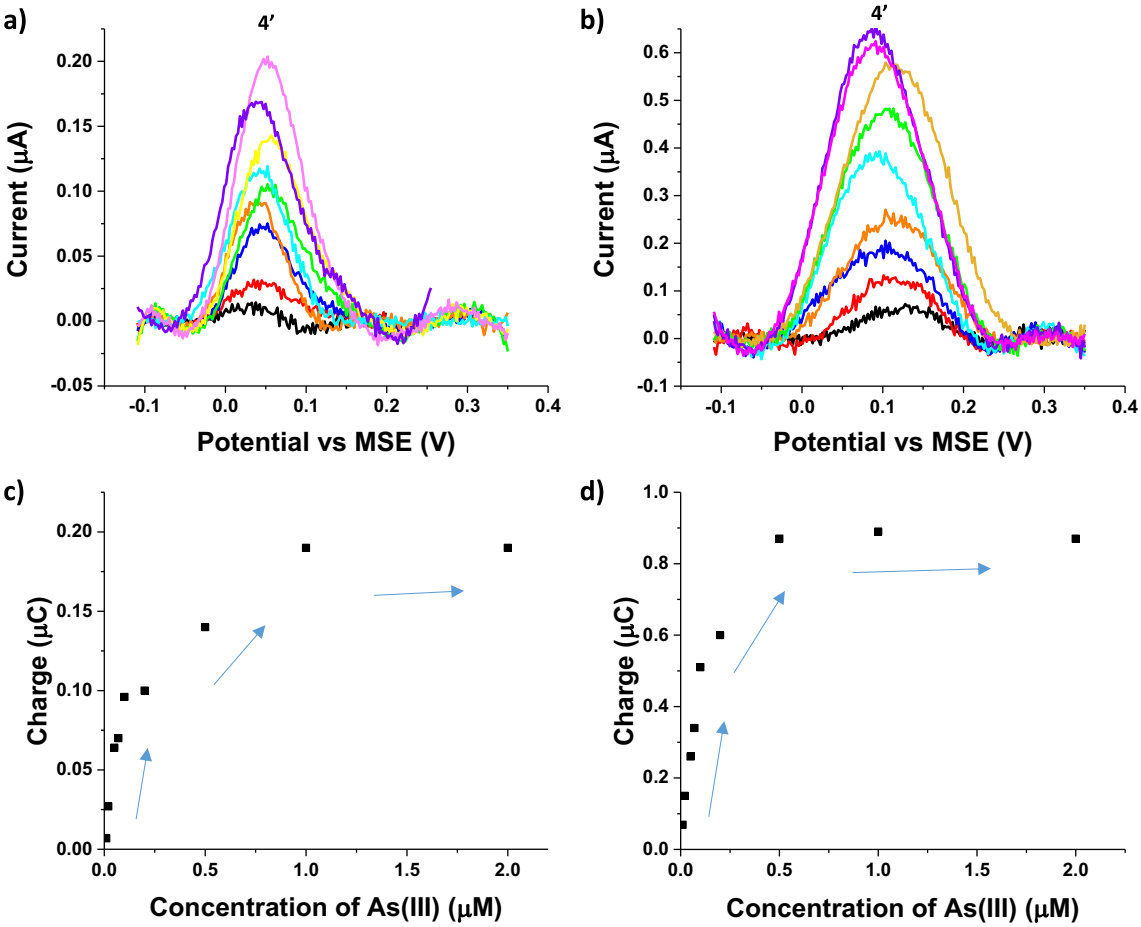

Fig. 3. Baseline corrected stripping voltammograms of various concentrations of As(III) in 0.1 M H_2SO_4 at a) Au macroelectrodes and b) Au nanoparticle-modified GCEs. Also shown are plots of the charge of peak 4′ vs concentrations of As(III) in 0.1 M H_2SO_4 at c) Au macroelectrodes and d) Au nanoparticle-modified GCEs. The concentrations of As(III) were 0.01 μM (black), 0.02 μM (red), 0.05 μM (blue), 0.07 μM (orange), 0.1 μM (cyan), 0.2 μM (green), 0.5 μM (yellow), 1 μM (purple), and 2 μM (pink). ASV parameters: deposition at − 0.9 V vs. MSE for 300 s, potential scan rate 0.1 V s^{-1}, and baseline was modelled via polynomial method from − 0.1 V to + 0.35 V for peak 4′. (For interpretation of the references to colour in this figure legend, the reader is referred to the web version of this article.)

sponds to an estimated coverage of ca 9.0 × 10^{13} molecules cm^{-2} and a deposition of 0.12 monolayers of As ad-atoms (See SI section 5 for sample calculations).

Based on the experimental results, there were less than one monolayer of As ad-atoms deposited onto the surface of Au even increasing the concentrations of As(III). The analytical measurements in this study were thus based on the measurement of sub-monolayer of deposited As(0) ad-atoms.

Although peak 4′ increased with the concentration of As(III) in the range of 0.01 μM to 1 μM or 0.01 μM to 0.5 μM for Au macroelectrodes and Au nanoparticle-modified electrodes, respectively, it is still necessary to find a linear range at low concentrations to approach a lower detection limit and a higher sensitivity. Further attention was thus focussed on the novel use of peak 4′ at lower concentrations of As(III).

5.2. Calibration curves and limits of detections

To further probe the linear range to assess the sensitivity and to identify a linear range and the detection limit, concentrations of As (III) below 0.1 μM were studied for both electrodes from an analytical perspective. The deposition time for ASV was optimized to be 300 s at Au macroelectrode in 0.1 μM As(III) as summarized in SI section 6 whilst the deposition potential for ASV was optimized to be – 0.9 V in 10 μM As(III) as summarized in SI section 7. Hence in the following, the pre-concentration was carried out at Au macroelectrodes with various concentrations of As(III) in 0.1 M H_2SO_4 at – 0.9 V for 300 s. Note that the previous literature focuses on the oxidation of bulk As(0) rather than As ad-atoms [31,42], and so did not require long deposition times but were unlikely to reach real detection limits compatible with the WHO limit, and in any case are prone to interference by Cu(II) ions. In this paper, we focus only on the As ad-atoms to reach the low detection limit and avoid interference from Cu ions but the deposition time is longer than those previous methods. Baseline corrections to peak 4′ were applied as above. Fig. 4a shows the baseline corrected stripping voltammograms of peak 4′ with the concentrations of As (III) from 0.01 μM to 0.1 μM at Au macroelectrodes. The peak 4′ was observed at ca + 0.05 V and the charge of the peak was increased with the concentrations of As(III) as shown in Table S1. To obtain the relationship between the charge of peak 4′ and the concentration of As (III) at Au macroelectrodes, the charges were plotted against the concentrations in Fig. 4c. A linear relationship, $Charge = 9.5 \times 10^{-7} C\mu M^{-1} \times [As(III)] + 4 \times 10^{-9} C$, was obtained between 0.01 μM and 0.1 μM, and the error bars were standard deviation calculated from at least three sets of data.

Rather than estimating the LOD using the popular method based on 3σ [45], which is known to give unrealistically low estimates for cali-

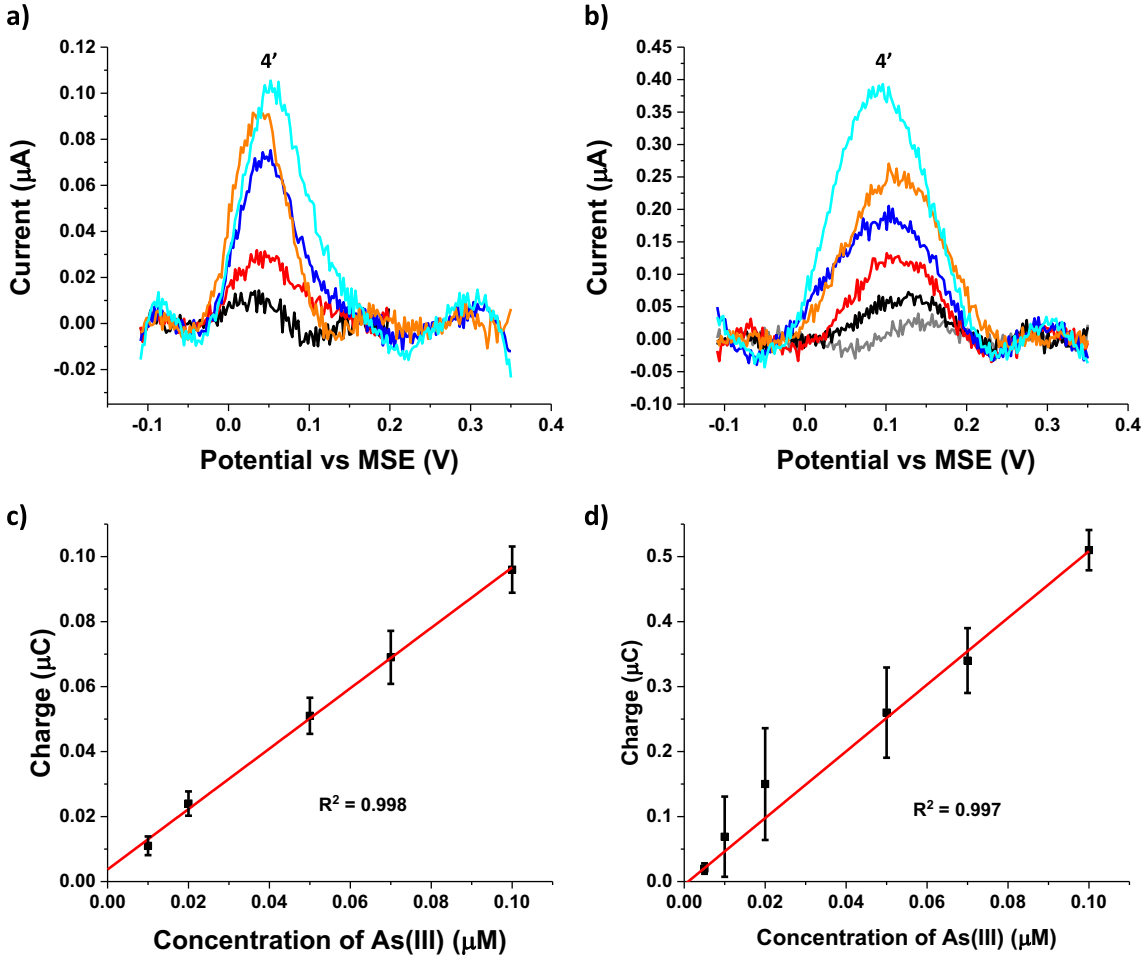

Fig. 4. Baseline corrected stripping voltammograms of various concentrations of As(III) in 0.1 M H_2SO_4 at a) Au macroelectrode and b) 5 nm Au nanoparticle-modified GC electrode. The concentrations of As(III) were 0.005 μM (grey), 0.01 μM (black), 0.02 μM (red), 0.05 μM (blue), 0.07 μM (orange) and 0.1 μM (cyan). Charge of stripped As(0) ad-atoms vs. the concentration of As(III) at c) Au macroelectrode and d) 5 nm Au nanoparticle-modified GC electrode. The charge was calculated from baseline corrected LSVs and the error bars shown are standard deviations calculated from at least three sets of data. ASV parameters: deposition at − 0.9 V vs. MSE for 300 s, potential scan rate 0.1 V s^{-1}, and baseline was modelled via polynomial method from − 0.1 V to + 0.35 V for peak 4′. (For interpretation of the references to colour in this figure legend, the reader is referred to the web version of this article.)

bration curves of high linearity since σ will be very small leading to a calculated extremely low detection limit. As Brett and Brett emphasise 'such a limit may not be attainable owing to limitations of the experimental procedure or the instrumentation (noise and drift at low signal levels), apart from any chemical interferences' [45]. For this reason, they recommend the use of 'practical detection limits' based on whether or not it is possible to distinguish the signal from the background. We adopt the latter approach in this paper and the visually identified LOD of 0.01 μM (0.8 ppb) with the sensitivity of 9.5×10^{-7}C μM^{-1} were acquired on Au macroelectrodes. Note that the quoted LOD is estimated on the basis of the visual identification of measureable signals (shown in SI section 3) from real samples (black line in Fig. 4c) rather than calculated based on the 3σ method. To further explore the analytical use of peak 4′, analogous experiments were made at Au nanoparticle-modified electrodes as follows.

The pre-concentration of As(0) was carried out at –0.9 V for 300 s in various concentrations of As(III) solution. Stripping used a linear sweep from –0.9 V to +0.62 V at a scan rate of 0.1 V s^{-1} at Au nanoparticle-modified GCEs. The baseline correction for peak 4′ is also followed the procedure as above. Fig. 4b presents the baseline corrected stripping voltammograms of peak 4′ at Au nanoparticle-modified GCEs which was obtained from 0.005 μM to 0.1 μM. Similar to that at Au macroelectrodes, the peak 4′ was observed at ca + 0.1 V and the charge was increased with the concentrations of As(III) (Table S1). The charges of peak 4′ vs concentrations of As(III) at Au nanoparticle-modified GCEs was plotted in Fig. 4d. The linear relationship, $Charge = 5.1 \times 10^{-6} C\mu M^{-1} \times [As(III)] - 5 \times 10^{-9} C$, was obtained from 0.005 μM to 0.1 μM, and the error bars were standard deviations calculated from at least three sets of data. As above, the LOD was judged based on the need to have a visually clear signal over background and found to be 0.005 μM (0.4 ppb). The grey line in Fig. 4b shows the voltammogram corresponding to this limit. The sensitivity was estimated to be 5×10^{-6}C μM^{-1}. In comparison with the results on Au macroelectrodes, a lower LOD and higher sensitivity was obtained at Au nanoparticle-modified GCEs, which suggest a merit of using Au nanoparticle-modified electrodes over Au macroelectrodes during application of As(III) detection in water. The enhancement is attributed to the greater surface area of Au available, which was estimated to be 0.2 cm^2 at Au nanoparticles (see SI section 1 for calculations) while 0.02 cm^2 at Au macroelectrodes (calculations shown in SI section 2).

The detection limits obtained using visually clear signals of 0.8 ppb and 0.4 ppb on Au macroelectrodes and Au nanoparticle-modified GCEs, respectively, meet the WHO guidelines for arsenic in drinking water (10 ppb). To apply this method in real world, interference study is also required. The next section will focus on the interference from Cu(II) and chloride.

6. Interference studies

Having established an analytical procedure based on the UPD stripping peak of As ad-atoms from gold surface, further experiments were conducted to explore if the detection on gold suffers interference from either copper or chloride as is discussed in this section.

6.1. Possible interference by Cu(II)

Cu(II) is a very common interferent in the stripping voltammetry of As using bulk As since it can form Cu-As alloys or intermetallic compounds in the deposition step [46]. Accordingly the interference of Cu(II) with detection of 0.1 μM of As(III) was studied using ASV by adding different amounts of Cu(II). The pre-concentration was conducted at – 0.9 V for 300 s with detection using a linear sweep, as above, from – 0.9 V to + 0.62 V at a scan rate of 0.1 V s^{-1}. Fig. 5a illustrates the raw ASV of 0.1 μM of As(III) with different amounts of Cu^{2+} from 0.1 μM to 1 mM at Au macroelectrodes. A peak observed at ca – 0.3 V and peak current was increased with the concentrations of Cu(II). This was assigned to the oxidation peak of Cu(0) to Cu(II) [47]. The peak 4′ at ca + 0.05 V was difficult to be seen thus a baseline corrections were made for peak 4′ with the procedure as above. Fig. 5c shows the baseline corrected stripping voltammograms of 0.1 μM of As(III) with different amounts of Cu^{2+} from 0.1 μM to 1 mM at Au macroelectrodes. The black dashed line was recorded for a solution without Cu(II) where only one peak was observed at ca + 0.05 V corresponding to the oxidation of As ad-atoms [42–44]. With the addition of Cu(II), the signal of peak 4′ varied negligibly and the peak potential did not shift. Even for concentrations of Cu(II) was as high as 1 mM, the signal of peak 4′ was not changed. Thus, it can be concluded that Cu(II) does not interfere to the oxidation peak of As ad-atoms on Au macroelectrodes.

Analogous experiments were made on Au nanoparticle-modified GCEs. The pre-concentration was carried out at – 0.9 V for 300 s then followed up with a linear sweep from – 0.9 V to + 0.62 V at a scan rate of 0.1 V s^{-1}. Fig. 5b illustrates the raw ASV of 0.1 μM of As(III) with different amounts of Cu^{2+} from 0.1 μM to 1 mM at Au nanoparticle-modified GCEs. Similar to what was seen at Au macroelelctrodes, a Cu^{2+} reduction peak can be observed at ca – 0.3 V and the associated peak current increased with the addition of Cu^{2+}. Baseline correction was applied for peak 4′ with the procedure as above and the baseline corrected ASV is shown in Fig. 5d. The peak 4′ can be observed at ca + 0.1 V and again the addition of Cu(II) did not change the signal of peak 4′ or shift the potential by comparing the voltammograms obtained without (black dashed line in Fig. 5d) and with Cu(II). In Fig. 5c and d, the peak at ca +0.25 V or ca +0.30 V was an artefact arising from the baseline correction. It does not relate to any Faradaic reaction. The baseline simulated in that range was based on the polynomial method optimised for the peak of interest and so does not perfectly capture the background outside of potential range of the ad-atom stripping peak. That causes a small peak shown in Fig. 5c and d at +0.25 V or +0.30 V, respectively. We conclude that the formation of Cu-As alloys or intermetallic species was likely avoided by using UPD to form As ad-atoms rather than bulk As at gold surfaces. The standard deviations of peak potential were calculated to be 0.010 and 0.015 for Au macroelectrodes and Au nanoparticle-modified electrodes, respectively, which means the difference of peak potentials in Fig. 5c and d were negligible.

6.2. Possible interference by chloride

Chloride ions are recognised as an interferent in As(III) detection on some metal surfaces such as Pt when using the ASV of bulk As and when using UPD-ASV with Platinum electrodes [8,35]. Thus, Chloride ions were also investigated in an interference study with different concentrations of Cl^-. The pre-concentrations were conducted at –0.9 V for 300 s with detection via a linear potential sweep from –0.9 V to +0.62 V at a scan rate of 0.1 V s^{-1}. Then the baseline correction was applied to peak 4′ with the procedure as above. Fig. 6a presents the baseline corrected stripping voltammograms obtained from 0.1 μM of As(III) in 0.1 M H_2SO_4 with the addition of Cl^- from 1 μM to 0.54 M at Au macroelectrodes. The black dashed line was recorded for a solution without Cl^- where only one peak was observed at ca + 0.05 V corresponding to the peak 4′. With the addition of Cl^-, the signal of peak 4′ varied negligibly. Even for concentrations of Cl^- was as high as 0.54 M, the signal of peak 4′ was not changed. Thus, it can be concluded that Cl^- does not interfere to the oxidation peak of As ad-atoms on Au macroelectrodes.

Analogous experiments were made on Au nanoparticle-modified GCEs. The pre-concentration was conducted at –0.9 V for 300 s with detection using a linear sweep from –0.9 V to +0.62 V at a scan rate of 0.1 V s^{-1}. Baseline corrections were also made for peak 4′ with the procedure as above. Fig. 6b displays the baseline corrected ASVs

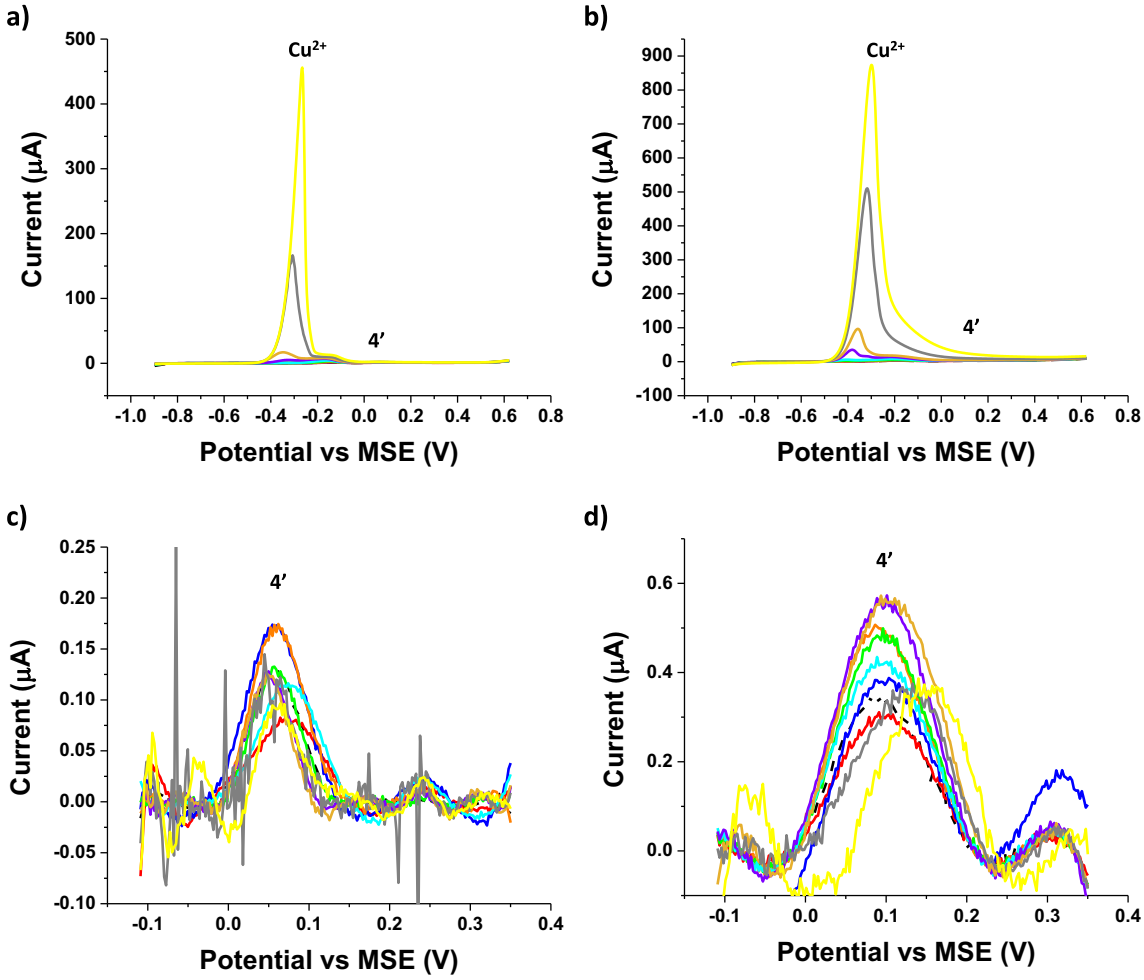

Fig. 5. Raw ASV curves of 0.1 μM As(III) in 0.1 M H_2SO_4 with various concentrations of Cu^{2+} at a) Au macroelectrodes and b) 5 nm Au nanoparticle-modified GC electrodes. Baseline corrected ASV curves of 0.1 μM As(III) in 0.1 M H_2SO_4 with various concentrations of Cu^{2+} in the potential range from − 0.1 V to + 0.35 V at c) Au macroelectrodes and d) Au nanoparticle-modified GC electrodes. ASV parameters: deposition at − 0.9 V for 300 s, scan rate was 0.1 V s^{-1}. Cu(II) concentration: 0 μM (black dashed line), 0.1 μM (red), 0.5 μM (blue), 1 μM (orange), 5 μM (green), 10 μM (cyan), 50 μM (purple), 100 μM (yellow), 500 μM (grey) and 1 mM (light yellow). (For interpretation of the references to colour in this figure legend, the reader is referred to the web version of this article.)

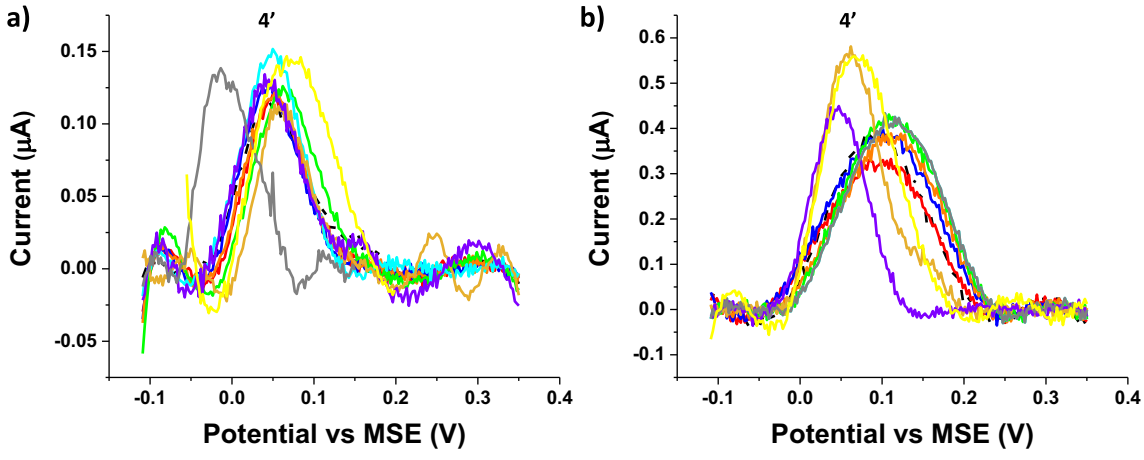

Fig. 6. Baseline corrected ASV curves of 0.1 μM As(III) in 0.1 M H_2SO_4 with various concentrations of Cl^- in the potential range from − 0.1 V to + 0.35 V at a) Au macroelectrodes and b) Au nanoparticle-modified GC electrodes. ASV parameters: deposition at − 0.9 V for 300 s, scan rate was 0.1 V s^{-1}. Cl^- concentrations: 0 μM (black dashed line), 1 μM (red), 5 μM (blue), 10 μM (orange), 50 μM (green), 100 μM (cyan), 7000 μM (yellow), 20 mM (purple), 100 mM (grey) and 0.54 M (light yellow). (For interpretation of the references to colour in this figure legend, the reader is referred to the web version of this article.)

obtained from 0.1 μM of As(III) with various concentrations of Cl^- from 1 μM to 0.54 M at Au nanoparticle-modified GCEs. Similar to what was seen at Au macroelectrodes, again the charge of peak 4′ at ca + 0.1 V did not change excessively with the addition of Cl^- as judged by comparison of the voltammograms obtained without (black dashed line in Fig. 6b) and with Cl^-. The results suggest that the method is free from interference by chloride.

6.3. Possible synergistic interference by Cu(II) and chloride

The above shows that Cu(II) and chloride do not separately influence the detection of As using the UPD ASV method so offering major advantages over either the use if bulk As for ASV or Pt electrodes for UPD ASV. However, it was deemed prudent to check if the simultaneous presence of both species had any influence at on As(III) detection at both types of electrodes. Pre-concentration was carried out at – 0.9 V for 300 s and detection with a linear sweep from – 0.9 V to + 0.62 V at a scan rate of 0.1 V s^{-1} in various concentrations of As(III) from 0.05 μM to 0.1 μM with the addition of 1 mM Cu^{2+} or 0.54 M Cl^- at Au macroelectrodes. Baseline corrections were then made and the charge was calculated with the procedures as above. Fig. 7a shows the charge of peak 4′ vs concentrations of As(III) obtained from 0.01 μM to 0.1 μM without interferents (black), with 1 mM Cu^{2+} (red), with 0.54 M Cl^- (blue), and with both 1 mM Cu^{2+} and 0.54 M Cl^- (green). The error bars were standard deviation calculated from at least three sets of data. All points with possible interferents are seen to lie within the error bars of the arsenic signal (black points in Fig. 7a). A linear line was simulated with all points in the plot (yellow line in Fig. 7a) with an equation of $Charge = 1.0 \times 10^{-6} C\mu M^{-1} \times [As(III)] + 1.6 \times 10^{-9} C$. Compare to the equation obtained in Fig. 4c, the sensitivity varied by no more than ca 5% from 9.5 × 10^{-7}C μM^{-1} to 1.0 × 10^{-6}C μM^{-1}. Thus, we conclude that there is no synergistic interference of either Cu^{2+} or Cl^- on the oxidation peak of As ad-atoms on Au macroelectrodes.

Similar experiments were also made on Au nanoparticle-modified GCEs. Pre-concentration was again carried out at – 0.9 V for 300 s and detection with a linear sweep from – 0.9 V to + 0.62 V at a scan rate of 0.1 V s^{-1} in various concentrations of As(III) from 0.05 μM to 0.1 μM with the addition of 1 mM Cu^{2+} or 0.54 M Cl^- at Au nanoparticle-modified GCEs. Baseline corrections were made and the charge was calculated with the procedures as above. Fig. 7b displays the charge of peak 4′ vs concentrations of As(III) obtained from 0.005 μM to 0.1 μM without interferents (black), with 1 mM Cu^{2+} (red), with 0.54 M Cl^- (blue), and with both 1 mM Cu^{2+} and 0.54 M Cl^- (green). The error bars were standard deviation calculated from at least three sets of data. All points lie within the error bars of the arsenic signal (black points in Fig. 7b). A linear line was simulated with all points in the plot (yellow line in Fig. 7b) with an equation of $Charge = 5.0 \times 10^{-6} C\mu M^{-1} \times [As(III)] - 4.3 \times 10^{-9} C$. Compare to the equation obtained in Fig. 4d, the sensitivity remained the same as 5.0 × 10^{-6}C μM^{-1}. Thus, it can be concluded that neither Cu^{2+} nor Cl^- interfere with the oxidation peak of As ad-atoms on Au surfaces. The sensitivity of the UPD ASV method is not affected by Cu^{2+} and Cl^- or combinations of them.

In comparison with previous methods for detecting As(III) under normal ASV conditions [42], bulk As(0) was deposited at gold surface at ca −0.7 V for 180 s, but did not show measurable stripping peaks for concentrations lower than 50 μM. Cu(II) was reported as the only likely interference in such measurements. As for UPD methods for detecting bulk As(III), Xiao *et al* used square wave voltammetry after deposited bulk As(0) at – 0.8 V for 120 s and calculated a LOD based on 3σ method of 0.1 ppb [31]. Neither method reported a visually clear detection limit as low as 10 ppb.

The significant issues of interference by copper and by chloride have been solved by using UPD ASV. To optimise the electrode used it is interesting to compare the time of measurement and cost of the different approaches and these data are shown in SI Section 8. The Au screen printed electrode has the lowest cost and the shortest time for each measurement (Table S2), which encourages the future use of disposable electrodes for real world applications.

7. Conclusions

The analytical use of underpotential deposition of As on gold surface with anodic stripping of the adsorbed As ad-atoms has been validated on both gold macroelectrodes and gold nanoparticle-modified electrodes. Limits of detection within the requirements by WHO guidelines for safe drinking water were observed at both electrodes with clearly visible signals in each case even at the lowest concentrations studied. A particular merit of using UPD-ASV method to detect As (III) using Au substrates is that it can avoid the interference from Cu^{2+} and Cl^- or combinations of them. The detection limit for gold

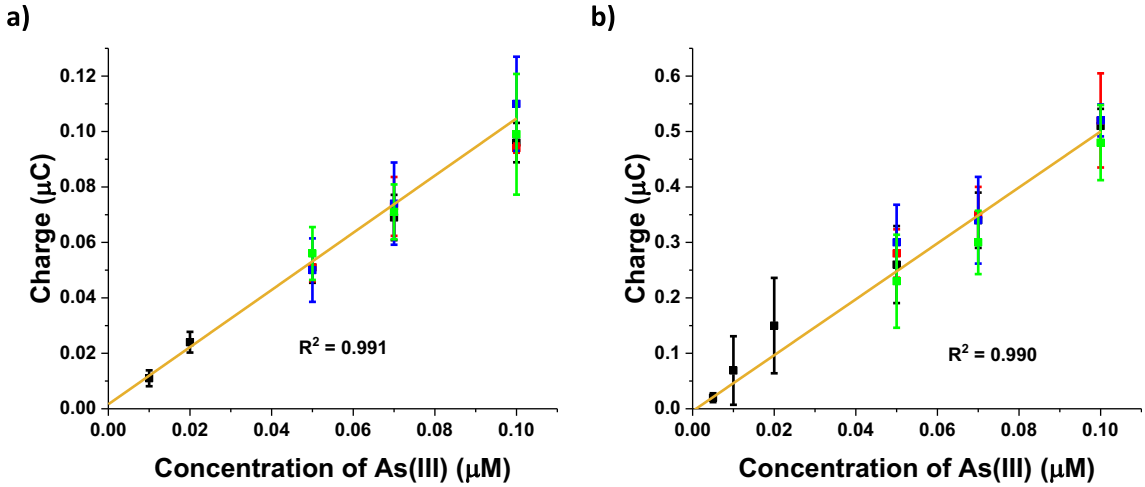

Fig. 7. Charge of stripped As(0) ad-atoms vs. the concentration of As(III) at a) Au macroelectrode and b) 5 nm Au nanoparticle-modified GC electrode. The points included were various concentrations of As(III) (black), As(III) solutions contained 1 mM Cu^{2+} (red), As(III) solutions contained 0.54 M Cl^- (blue), and As(III) solutions contained both 1 mM Cu^{2+} and 0.54 M Cl^- (green). The charge was calculated from baseline corrected LSVs and error bars were standard deviations calculated from at least sets of data. The calibration lines (yellow) were calculated based on the charges of all points in the graphs. LSV parameters: deposition at − 0.9 V vs. MSE for 300 s, potential scan rate 0.1 V s^{-1}. (For interpretation of the references to colour in this figure legend, the reader is referred to the web version of this article.)

nanoparticle-modified electrodes was lower and the sensitivity was higher than gold macroelectrodes, which offers particular benefit in using nanoparticle-modified electrodes over macroelectrodes.

CRediT authorship contribution statement

Yifei Zhang: Formal analysis, Investigation, Writing – original draft. **Danlei Li:** Data curation. **Richard G. Compton:** Writing – review & editing, Supervision, Project administration.

Declaration of Competing Interest

The authors declare that they have no known competing financial interests or personal relationships that could have appeared to influence the work reported in this paper.

Appendix A. Supplementary data

Supplementary data to this article can be found online at https://doi.org/10.1016/j.jelechem.2022.116154.

References:

[1] J. Wang, Analytical Electrochemistry, Wiley-VCH2006.
[2] Allen J. Bard, L.R. Faulkner, Electrochemical Methods: Fundamentals and Applications, 2nd ed., John Wiley & Sons, Inc, New York, 2001.
[3] C. Brett, A.M. Oliveira Brett, Electrochemistry: principles, methods, and applications, 1993.
[4] A.J. Borrill, N.E. Reily, J.V. Macpherson, Addressing the practicalities of anodic stripping voltammetry for heavy metal detection: a tutorial review, Analyst 144 (23) (2019) 6834–6849.
[5] M. Fleischmann, S. Pons, The behavior of microelectrodes, Anal. Chem. 59 (24) (1987) 1391A–1399A.
[6] C. He, M. Tao, C. Zhang, Y. He, W. Xu, Y. Liu, W. Zhu, Microelectrode-based electrochemical sensing technology for in vivo detection of dopamine: recent developments and future prospects, Crit. Rev. Analyt. Chem. (2020) 1–11.
[7] R.G. Compton, G.G. Wildgoose, N.V. Rees, I. Streeter, R. Baron, Design, fabrication, characterisation and application of nanoelectrode arrays, Chem. Phys. Lett. 459 (1-6) (2008) 1–17.
[8] Y. Zhang, D. Li, R.G. Compton, Arsenic, ChemElectroChem 8 (19) (2021) 3707–3715.
[9] L. Bu, J. Liu, Q. Xie, S. Yao, Anodic stripping voltammetric analysis of trace arsenic (III) enhanced by mild hydrogen-evolution at a bimetallic Au-Pt nanoparticle modified glassy carbon electrode, Electrochem. Commun. 59 (2015) 28–31.
[10] Z. Guo, M. Yang, X.-J. Huang, Recent developments in electrochemical determination of arsenic, Curr. Opin. Electrochem. 3 (1) (2017) 130–136.
[11] M. Dali, K. Zinoubi, A. Chrouda, S. Abderrahmane, S. Cherrad, N. Jaffrezic-Renault, A biosensor based on fungal soil biomass for electrochemical detection of lead (II) and cadmium (II) by differential pulse anodic stripping voltammetry, J. Electroanal. Chem. 813 (2018) 9–19.
[12] A. Nsabimana, S.A. Kitte, T.H. Fereja, M.I. Halawa, W. Zhang, G. Xu, Recent developments in stripping analysis of trace metals, Curr. Opin. Electrochem. 17 (2019) 65–71.
[13] E. Desimoni, F. Palmisano, L. Sabbatini, Simultaneous determination of tin and lead at the parts-per-billion level by coupling differential pulse anodic stripping voltammetry with a matrix exchange method, Anal. Chem. 52 (12) (1980) 1889–1892.
[14] J. Orozco, C. Fernández-Sánchez, C. Jiménez-Jorquera, Underpotential deposition-anodic stripping voltammetric detection of copper at gold nanoparticle-modified ultramicroelectrode arrays, Environ. Sci. Technol. 42 (13) (2008) 4877–4882.
[15] C.A. Paddon, R.G. Compton, Underpotential deposition of lithium on platinum single crystal electrodes in tetrahydrofuran, J. Phys. Chem. C 111 (26) (2007) 9016–9018.
[16] O.A. Oviedo, L. Reinaudi, S.G. García, E.P.M. Leiva, Underpotential deposition, Monogr. Electrochem. (2016).
[17] F.J. Sarabia, V. Climent, J.M. Feliu, Underpotential deposition of Nickel on platinum single crystal electrodes, J. Electroanal. Chem. 819 (2018) 391–400.
[18] L.Y. Wang, X.L. Peng, H.J. Fu, C. Huang, Y.P. Li, Z.M. Liu, Recent advances in the development of electrochemical aptasensors for detection of heavy metals in food, Biosens. Bioelectron. 147 (2020) 10.
[19] D. Banik, S.K. Manna, A.K. Mahapatra, Recent development of chromogenic and fluorogenic chemosensors for the detection of arsenic species: Environmental and biological applications, Spectroc. Acta Pt. A-Molec. Biomolec. Spectr. 246 (2021) 19.
[20] K. Mao, H. Zhang, Z.L. Wang, H.R. Cao, K.K. Zhang, X.Q. Li, Z.G. Yang, Nanomaterial-based aptamer sensors for arsenic detection, Biosens. Bioelectron. 148 (2020) 15.
[21] X.C. Xu, X.H. Niu, X. Li, Z.H. Li, D. Du, Y.H. Lin, Nanomaterial-based sensors and biosensors for enhanced inorganic arsenic detection: a functional perspective, Sens. Actuator B-Chem. 315 (2020) 13.
[22] S. Sikdar, M. Kundu, A review on detection and abatement of heavy metals, ChemBioEng Rev. 5 (1) (2018) 18–29.
[23] X.P. Yu, C.L. Liu, Y.F. Guo, T.L. Deng, Speciation analysis of trace arsenic, mercury, selenium and antimony in environmental and biological samples based on hyphenated techniques, Molecules 24 (5) (2019) 23.
[24] S. Li, C. Zhang, S. Wang, Q. Liu, H. Feng, X. Ma, J. Guo, Electrochemical microfluidics techniques for heavy metal ion detection, Analyst 143 (18) (2018) 4230–4246.
[25] G.M. dos Santos, D. Pozebon, C. Cerveira, D.P. de Moraes, Inorganic arsenic speciation in rice products using selective hydride generation and atomic absorption spectrometry (AAS), Microchem. J. 133 (2017) 265–271.
[26] I. Komorowicz, A. Hanć, W. Lorenc, D. Barałkiewicz, J. Falandysz, Y. Wang, Arsenic speciation in mushrooms using dimensional chromatography coupled to ICP-MS detector, Chemosphere 233 (2019) 223–233.
[27] H. Cheng, W. Zhang, Y. Wang, J. Liu, Graphene oxide as a stationary phase for speciation of inorganic and organic species of mercury, arsenic and selenium using HPLC with ICP-MS detection, Microchim. Acta 185 (9) (2018) 1–8.
[28] B. Bansod, T. Kumar, R. Thakur, S. Rana, I. Singh, A review on various electrochemical techniques for heavy metal ions detection with different sensing platforms, Biosens. Bioelectron. 94 (2017) 443–455.
[29] K. Pungjunun, S. Chaiyo, I. Jantrahong, S. Nantaphol, W. Siangproh, O. Chailapakul, Anodic stripping voltammetric determination of total arsenic using a gold nanoparticle-modified boron-doped diamond electrode on a paper-based device, Microchim. Acta 185 (7) (2018) 1–8.
[30] A. Profumo, D. Merli, M. Pesavento, Voltammetric determination of inorganic As (III) and total inorganic As in natural waters, Anal. Chim. Acta 539 (1-2) (2005) 245–250.
[31] L. Xiao, G.G. Wildgoose, R.G. Compton, Sensitive electrochemical detection of arsenic (III) using gold nanoparticle modified carbon nanotubes via anodic stripping voltammetry, Anal. Chim. Acta 620 (1-2) (2008) 44–49.
[32] J.-H. Hwang, P. Pathak, X. Wang, K.L. Rodriguez, J. Park, H.J. Cho, W.H. Lee, A novel Fe-Chitosan-coated carbon electrode sensor for in situ As(III) detection in mining wastewater and soil leachate, Sens. Actuator B-Chem. 294 (2019) 89–97.
[33] C. Nunez, J.J. Trivino, R. Segura, V. Arancibia, Monographs in Electrochemistry trace levels in urine by differential pulse anodic voltammetry using a simple graphene screen-printed electrode, Microchem. J. 159 (2020) 6.
[34] A.O. Idris, J.P. Mafa, N. Mabuba, O.A. Arotiba, Dealing with interference challenge in the electrochemical detection of As (III)—a complexometric masking approach, Electrochem. Commun. 64 (2016) 18–20.
[35] D.M. Novak, B.E. Conway, Competitive adsorption and state of charge of halide-ions in monolayer oxide film growth-processes at Pt anaodes, J. Chem. Soc. Faraday Trans. 77 (1981) 2341–2359.
[36] M. Yang, P.-H. Li, W.-H. Xu, Y. Wei, L.-N. Li, Y.-Y. Huang, Y.-F. Sun, X. Chen, J.-H. Liu, X.-J. Huang, Reliable electrochemical sensing arsenic(III) in nearly groundwater pH based on efficient adsorption and excellent electrocatalytic ability of AuNPs/CeO2-ZrO2 nanocomposite, Sens. Actuator B-Chem. 255 (2018) 226–234.
[37] M. Yang, P.-H. Li, W.-H. Xu, Y. Wei, L.-N. Li, Y.-Y. Huang, Y.-F. Sun, X. Chen, J.-H. Liu, X.-J. Huang, Reliable electrochemical sensing arsenic (III) in nearly groundwater pH based on efficient adsorption and excellent electrocatalytic ability of AuNPs/CeO2-ZrO2 nanocomposite, Sens. Actuators, B 255 (2018) 226–234.
[38] Gold Nanoparticles: Properties and Applications. https://www.sigmaaldrich.com/GB/en/technical-documents/technical-article/materials-science-and-engineering/biosensors-and-imaging/gold-nanoparticles.
[39] J. Wei, S.-S. Li, Z. Guo, X. Chen, J.-H. Liu, X.-J. Huang, Adsorbent assisted in situ electrocatalysis: an ultra-sensitive detection of As (III) in water at Fe3O4 nanosphere densely decorated with Au nanoparticles, Anal. Chem. 88 (2) (2016) 1154–1161.
[40] A. Buffa, D. Mandler, Arsenic(III) detection in water by flow-through carbon nanotube membrane decorated by gold nanoparticles, Electrochim. Acta 318 (2019) 496–503.
[41] L. Bu, T. Gu, Y. Ma, C. Chen, Y. Tan, Q. Xie, S. Yao, Enhanced cathodic preconcentration of As (0) at Au and Pt electrodes for anodic stripping voltammetry analysis of As (III) and As (V), J. Phys. Chem. C 119 (21) (2015) 11400–11409.
[42] X. Dai, O. Nekrassova, M.E. Hyde, R.G. Compton, Anodic stripping voltammetry of arsenic (III) using gold nanoparticle-modified electrodes, Anal. Chem. 76 (19) (2004) 5924–5929.
[43] A. Buffa, D. Mandler, Arsenic (III) detection in water by flow-through carbon nanotube membrane decorated by gold nanoparticles, Electrochim. Acta 318 (2019) 496–503.
[44] D. Wang, Y. Zhao, H. Jin, J. Zhuang, W. Zhang, S. Wang, J. Wang, Synthesis of Au-decorated tripod-shaped Te hybrids for applications in the ultrasensitive detection of arsenic, ACS Appl. Mater. Interfaces 5 (12) (2013) 5733–5740.
[45] C.M.A. Brett, A.M.O. Brett, Electroanalysis, Oxford Science Publications1998.
[46] A. Jimana, M.G. Peleyeju, L. Tshwenya, K. Pillay, O.A. Arotiba, Voltammetric analysis of As(III) at a cobalt nanoparticles/reduced graphene oxide modified exfoliated graphite electrode, Int. J. Electrochem. Sci. 13 (11) (2018) 10127–10140.
[47] C. Gao, X.-Y. Yu, S.-Q. Xiong, J.-H. Liu, X.-J. Huang, Electrochemical detection of arsenic (III) completely free from noble metal: Fe3O4 microspheres-room temperature ionic liquid composite showing better performance than gold, Anal. Chem. 85 (5) (2013) 2673–2680.